The challenge of integrating offshore wind power in the U.S. electric grid. Part I: Wind forecast error.

C. L. Archer[1], H. P. Simão[2], W. Kempton[1], W. B. Powell[2], and M. J. Dvorak[3]

[1]College of Earth, Ocean, and Environment, University of Delaware

[2]Department of Operations Research and Financial Engineering, Princeton University

[3]Sailor's Energy, Vallejo, California

Corresponding author: Cristina L. Archer, University of Delaware, Integrated Science and Engineering Laboratory (ISELab) #371, 221 Academy Street, Newark, DE 19716, USA, carcher@udel.edu, +1 302 831 6640

Keywords: wind power, offshore wind power, weather prediction, forecast error.

Highlights:

1. The offshore wind resource along the U.S. East Coast is modeled at increasing build-out levels with consideration of conflicting water uses and exclusion zones;
2. A stochastic model of the offshore wind power forecast error was developed and calibrated based on current, existing, onshore wind farms;
3. Forty-eight hour forecasts of wind power at 5-km horizontal resolution and 10-minute temporal resolution are generated daily with a numerical weather prediction model for subsequent use in the unit commitment, economic dispatch, and power flow models in Part II.

Word count: 6608

Abstract

The purpose of this two-part study is to analyze large penetrations of offshore wind power into a Regional Transmission Organization (RTO) using realistic wind power forecast errors and a complete model of the RTO's unit commitment, economic dispatch, and power flow. The chosen RTO is PJM Interconnection, one of the largest independent system operators in the U.S. with a generation capacity of 186 Gigawatts (GW). The offshore wind resource along the U.S. East Coast is modeled at five build-out levels, varying between 7 and 70 GW of installed capacity, considering exclusion zones and conflicting water uses.

This paper, Part I of the study, describes in detail the wind forecast error model; the accompanying Part II describes the modeling of PJM's sequencing of decisions and information, inclusive of day-ahead, hour-ahead, and real-time commitments to energy generators with the Smart-ISO simulator and discusses the results.

Wind forecasts are generated with the Weather Research and Forecasting (WRF) model, initialized every day at local noon and run for 48 hours to provide midnight-to-midnight forecasts for one month per

season. Due to the lack of offshore wind speed observations at hub height along the East Coast, a stochastic forecast error model for the offshore winds is constructed based on forecast errors at 23 existing PJM inland wind farms. PJM uses an advanced, WRF-based forecast system with continuous wind farm data assimilation. The implicit (and conservative) assumption here is that the future forecast system for offshore winds will have the same performance as the current PJM's forecast system for inland winds, thus no advances in weather forecasting techniques are assumed.

Using the auto-regressive moving-average (ARMA) model, 21 equally-plausible sample paths of wind power forecast errors are generated and calibrated for each season at a control inland wind farm, chosen because of its horizontally uniform landscape and large size. The spatial correlation between pairs of inland wind farms is estimated with an exponential function and the matrix of error covariance is obtained. Validation at the control farm and at all other inland farms is satisfactory. The ARMA model for the wind power forecast error is then applied to the offshore wind farms at the various build-out levels and combined with the matrix of error covariance to generate multiple samples of forecast errors at the offshore farms. The samples of forecast errors are lastly added to the WRF forecasts to generate multiple samples of synthetic actuals of offshore wind power for use in Part II.

1 Introduction

As wind power and other types of variable electric generation develop, the integration of increasingly larger amounts of variable power into the electric grid is expected to become more challenging to manage. Integration becomes more difficult as the amount of wind power injected into the grid increases and as its variability increases. In contrast, integration is easier when wind farms are spread over larger geographic areas, which reduces variability caused by local weather patterns, and as the accuracy of the wind power forecasts is improved. In order to analyze these competing effects, we study one region and one wind resource in detail, i.e., offshore wind as an electricity resource for loads on the grid of the U.S. East Coast.

The U.S. East Coast is of interest because it includes numerous, large load centers and because the only large-scale, renewable energy source that is abundant, near cost-competitive, and close to load centers is offshore wind (Kempton et al. 2007; Department of Energy 2008; Sheridan et al. 2012; Dvorak et al. 2012, 2013). As of this writing, numerous projects are being proposed, with one under construction near Block Island off the state of Rhode Island. The aforementioned studies report on the large size of the offshore wind resource available, but have not been accompanied by studies showing how much of that can be integrated and how that integration would be achieved. The integration of wind power is challenging because of two fundamental characteristics of the wind:

1. Wind is fluctuating over all temporal horizons: seasonally (e.g., winds are generally higher in the winter than in the summer at mid-latitudes); weekly (e.g., windier conditions during synoptic-scale storms can last a few days to a week); daily (e.g., for inland wind turbines, higher winds are often observed at night than during the day at the hub height of modern turbines, >100 m, although the diurnal effect is reduced for turbines further offshore (Garvine and Kempton 2008)); and hourly or sub-hourly (e.g., turbulent fluctuations and gusts). The challenge is that these wind fluctuations are

not well correlated with the load (or demand), which therefore needs to be ultimately covered with other more controllable, and inevitably more polluting, energy sources, such as coal or natural gas;

2. Wind has limited predictability because, even with advanced numerical weather prediction models and with numerous observations, the atmospheric system is intrinsically non-linear and chaotic and therefore small errors in initial conditions or in numerical approximations can cause the predictions to diverge dramatically from the observations in just a few days (Lorenz 1963). In addition, the short-term range (<1-2 hours ahead) may be more challenging to predict than the medium-term (6-12 hours) and persistence still outperforms most other models (Ahlstrom et al. 2013, Foley et al. 2013).

Increasing the geographical dispersion of wind farms has been proven to be an effective method to ameliorate (but not eliminate) the first challenge, i.e., wind variability. The first U.S.-scale study of the benefits of interconnecting wind farms was conducted by Archer and Jacobson (2007) over the continental U.S. using observations. They found that wind power variability, expressed as the coefficient of variation, was improved if more and more wind farms were interconnected via transmission lines from distant locations. Similar findings were reported for: the offshore winds along the U.S. East Coast (Kempton et al. 2007; Kempton et al. 2010; Dvorak et al. 2012; Budischak et al. 2013), Texas (Katzenstein et al. 2010), the island of Corsica in the Mediterranean Sea (Cassola et al. 2008), and the western U.S. (Degeilh et al. 2011), among others (Sovacool 2008, Hart et al. 2012). Apt and Jaramillo (2014) have systematized the finding of smoothing by long distance, finding good agreement of their model with data. Based on this earlier research, to minimize wind variability, the offshore wind farms in this study will be geographically dispersed over a large swath of ocean and interconnected via under-water, high-voltage, direct-current (HVDC hereafter) transmission lines, as described in the next section.

The second challenge, i.e., the limited predictability of wind, is also impossible to eliminate. Weather forecasts have steadily improved in accuracy and timing with the advent of Numerical Weather Prediction (NWP) models, which simulate the complex phenomena that affect weather patterns (such as precipitation, turbulence, and interactions between land and sea) at fine spatial and temporal resolutions. However, since the atmosphere is a chaotic system (Lorenz 1963), it cannot be fully predicted via deterministic forecasts and therefore most weather offices today have adopted probabilistic approaches for NWP. One such probabilistic approach is the creation of several "ensembles," or sets of plausible future states of the atmosphere, which can then be used to estimate the probability distribution of the forecasted atmospheric variables of interest. Ensembles are created from the outputs of deterministic NWP models using either various initial conditions, different parameterizations or numerical schemes, or different NWP models. In general ensemble statistics have better accuracy than any individual deterministic ensemble member (Leith 1974; Molteni et al. 1996; Toth and Kalnay 1993, 1997; Krishnamurti et al. 2000; Kalnay 2003; Hirschberg et al. 2011), also for wind energy applications (Marquis et al. 2011; Archer et al. 2014; Delle Monache and Alessandrini 2014). However, generating enough ensemble members and over periods of time that are long enough to be representative of the variability of the wind forecast error can be computationally prohibitive.

An alternative to ensemble forecasting is to model the wind forecast error (not the wind) using a stochastic approach, for example with the auto-regressive moving-average (ARMA) model (Soder 2004;

Ummels et al. 2007; Naimo 2014). Given multi-weekly time series of actual wind forecast errors, expressed as the difference between actual wind power production and a forecast obtained with a deterministic NWP model, the ARMA model can generate, with small computational efforts, numerous sample paths of the wind forecast error that differ from the original time series but retain the same probabilistic properties, such as the variance of the error and the distribution of the length of the crossing-time distributions, capturing the time that the actual and simulated sample paths are above or below the forecast. These equally-plausible sample paths of forecast error can then be used to test planning strategies and assess the performance of an electric power system model fully inclusive of wind variability and forecast error. Note that ensembles and sample paths are different. Each ensemble member has its own performance and error distribution but they all attempt to reproduce the same wind event, whereas each sample path has the same performance and error properties as the original but represents a different (but equally likely) wind event. Because of its computational advantages, in this study we obtain estimates of the offshore wind forecast errors using ARMA sample paths (Part I) and then use the sample paths to tune a robust planning and scheduling policy to study the integration of large amounts of offshore wind in the electric grid (in Part II).

The research question addressed in this study combines both challenges together – wind variability and predictability – as follows: How much wind power, with its variability and forecast uncertainty fully accounted for, can be integrated within a current, large, and complex electric system, without making any changes to current forecasting techniques, reserve management, and transmission? We address this question using only current power system practice, that is, no new types of resources are introduced and no large-scale, fast-response storage is added.

A few technical feasibility studies have partially addressed this question by setting a target level of wind penetration defined by policy, then testing whether that amount can be integrated without major change. These studies, the major limitation of all of which is that they did not account for the wind forecast uncertainty in the planning process, are:

- The “20% by 2030” was the first study on wind integration at the national scale conducted by the U.S. Department of Energy (DOE) in 2008 (DOE 2008) in collaboration with industry, government, the National Renewable Energy Laboratory (NREL), and Lawrence Berkeley National Laboratory. A penetration of 20% in 2008 corresponded to about 305 GW (of which 50 GW offshore). Inclusive of transmission expansion costs, the report concluded that the benefits of adding about 300 GW of wind (50 GW of which offshore) in terms of greenhouse gas emission reduction, water conservation, and energy security would come at a high front-end capital cost, but not much higher cost of energy than from conventional generators (e.g., only 2% higher in the optimistic scenario). The report only accounted for wind forecast uncertainty indirectly as an added cost to the system: “system operating cost increases arising from wind variability and uncertainty amounted to about 10% or less of the wholesale value of the wind energy”.
- The Western Wind and Solar Integration Study (WWSIS, GE Energy 2010) focused on the WestConnect area and analyzed a portfolio of wind, solar photovoltaic, and concentrated solar power at penetrations of 11%-35%. The report indicates that a 35% energy penetration of wind and solar is feasible, but will require new operational strategies to better utilize existing technologies.

- The Eastern Wind Integration and Transmission Study (EWITS, EnerNex Corporation 2011) performed a similar analysis for the Eastern Interconnect and found that scenarios with penetrations of wind energy up to 30% were feasible if long-distance and high-capacity transmission infrastructure was constructed to improve balancing area cooperation.
- Budischak et al. (2013), rather than setting a mid-level, set several renewable energy penetration levels (30%, 40%, 90%) and determined how much over-generation and/or storage was optimal to operate the system with minimal cost neglecting existing baseload generation.
- The Eastern Renewable Generation Integration Study (ERGIS), conducted by NREL as a follow-on to the previous WWSIS and EWITS studies. Expected to be completed in 2015, it includes a day-ahead unit commitment model, 5-minute real-time dispatch, and a nodal DC-power flow model. More details are available at http://www.nrel.gov/electricity/transmission/eastern_renewable.html
- The National Offshore Wind Energy Grid Interconnection Study (NOWEGIS) was funded by the U.S. Department of Energy (DOE) and focuses specifically on offshore wind. It finds that 54 GW of offshore wind energy can be integrated in the U.S. grid by 2030, bringing a national reduction of annual production costs of $7.68 billion, resulting in an approximate value of offshore wind at $41/MWh. More details are available at http://energy.gov/eere/downloads/national-offshore-wind-energy-grid-interconnection-study-nowegis

Our study improves upon the ones above in several aspects. First, we use a realistic resource model, with offshore areas buildable with current-technology turbines (water depth limited to 60 m) and excluding areas of conflicting uses. We use a detailed weather model at high-temporal resolution to capture sub-hourly variations that might cause integration issues, combined with a long-distance HVDC line, so that power can be injected with minimal losses. We have developed and use here a combined unit commitment and power flow model, called "Smart-ISO," which uses detailed parameters for power plant operation and transmission grid capacity. Our Smart-ISO model, described in detail in Part II, carefully models the sequencing of decisions and information, including day-ahead, hour-ahead, and real-time commitments to energy generators, closely following the planning process used by PJM Interconnection. Special care was taken to model the fine-grained variability of energy from wind at higher penetration levels so that we capture the limits of ramp rates of different generators, given the notification times.

2 Wind power forecasts and synthetic actuals

2.1 PJM domain and offshore wind build-out levels

To address our research question, we modeled the planning process used by the PJM Interconnection RTO[1]. PJM is one of the largest RTOs in the U.S., with a territory that covers 14 states, 60 million people, and almost 60,000 miles of transmission lines. The PJM peak electricity demand in 2012 was 164 GW and the generation capacity was 186 GW (PJM 2012), including 72 GW of coal, 53 GW of natural gas, 34 GW of nuclear, and 0.9 GW from 55 inland wind farms (http://www.pjm.com/about-pjm/renewable-dashboard/renewables-today.aspx). PJM covers a large part of the U.S. East Coast, which is one of the

[1] RTOs in other areas are also referred to as Independent System Operator – ISO – or Transmission System Operator – TSO.

most promising offshore wind areas in the world (Archer and Jacobson 2003, 2005; Kempton et al. 2007; Dvorak et al. 2012, 2013; Archer et al. 2014). In addition, the Atlantic Wind Connection has proposed to build an underwater, high-voltage, DC transmission line between New York and Virginia, with several connection points in the PJM domain. Our model includes an HVDC line like this proposed one, drawing on their planned points of interconnection. In summary, PJM covers an excellent area to study the issue of the integration of large amounts of offshore wind power into the electric grid.

We analyze five build-out levels of offshore wind in PJM, summarized in Table I. The installed capacities were obtained with 90-m wind speed data from Dvorak at al. (2013) assuming 5-MW REpower wind turbines with a spacing of 10D x 10D (where D is the turbine rotor's diameter of 126 m), after applying array and electrical losses. The average output and the corresponding percentage of average PJM load represented by this output were obtained through the analysis reported in Part II of this paper (Simão et al. 2014).

The five build-out levels were established as follows. The first build-out level coincides with the current Wind Energy Areas (WEAs) leased out by the Bureau of Ocean Energy Management (BOEM) off the states of New Jersey, Delaware, Maryland and Virginia, with a total installed capacity of 7.3 GW and an average power production of 3.3 GW (thus a capacity factor of 45%), corresponding to 4.4% of the PJM average load in 2010. The next build-out levels have incrementally higher penetrations, all the way to the fifth one, with 69.7 GW of installed wind capacity, providing on average 42% of the PJM load (Table I). Offshore areas with conflicts were excluded, such as designated shipping lanes, military restricted zones, fish havens, areas with visual conflicts, dumpsites, or harbor restricted areas (Figure 1a). The remaining areas of no conflict were divided into 29 geographically contiguous blocks of 1 to 4.5 GW each. The individual blocks are designated by a digit, which refers to the build-out level, and a decimal, which indicates consecutive blocks generally in the north-south direction (e.g. 2.1, 2.2, 2.3 etc.). A map showing the location of the blocks used for the five build-out levels is shown in Figure 1b.

Table I: The five build-out levels of offshore wind considered in this study.

Build-out level	Blocks included (Figure 1)	N. of wind turbines	Installed capacity (GW)	Average output (GW)	Percent of average PJM load
1	1.1-1.4	1,638	7.3	3.3	4.4%
2	2.1-2.8	5,637	25.3	11.2	15.0%
3	3.1-3.4	7,990	35.8	16.0	21.4%
4	4.1-4.6	10,906	48.9	21.9	29.1%
5	5.1-5.7	15,556	69.7	31.5	42.0%

a

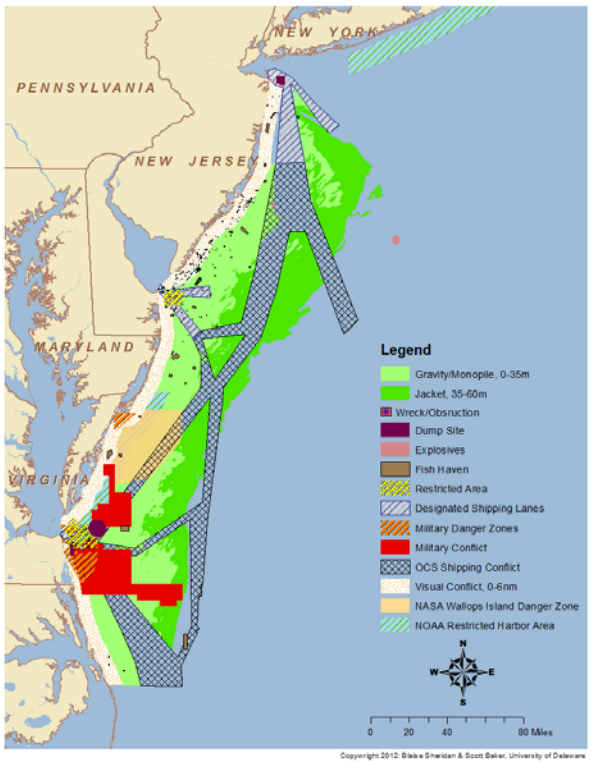

b

Figure 1: Maps of: a) conflicting use areas and b) blocks that are part of the five build-out levels described in Table I. The 2005-2010 average capacity factor based on 90-m wind speed from Dvorak et al. (2013) is color shaded in b). The locations of six buoys and a 43-m meteorological tower at the mouth of the Chesapeake Bay (CHLV2) are shown with a pin in b).

2.2 Synthetic actual winds

We use the Weather Research and Forecasting Model-Advanced Research (WRF-ARW, hereafter simply WRF) to generate the wind forecasts. WRF is a publicly developed and maintained, non-hydrostatic weather model capable of simulating global-to-microscale atmospheric conditions (Skamarock et al. 2008).

Forecast errors are usually obtained as the difference between the actual, in-situ wind observations, hereafter referred to as the "actuals," and the forecast model values, in our case the WRF-forecasted wind speed (or wind power). In order to reduce the errors, improvements are generally incorporated in the forecast model formulation, setup, initialization, numerical solvers, or model parameterizations. In this study, however, we have no actuals at all, because no observations of hub-height wind speed or power exist over the U.S. Eastern continental shelf, or along the shoreline. As such, we cannot calculate the error, because we have the forecasts from WRF but not the actuals to compare them against. The lack of adequate wind speed observations has been identified already as one of the main obstacles to the development of offshore wind farms along the U.S. East Coast by Archer et al. (2014) and references within it.

To overcome the lack of offshore wind actuals, we propose here a method that reverses the traditional forecast approach by providing estimates of the offshore actuals based on a combination of the WRF offshore forecasts and the forecast error observed at the inland (or onshore) wind farms operating in the PJM territory during 2013. The synthetic actuals obtained through this method will be referred to from here on as "onshore-based actuals." It may seem odd to "generate" actual wind data, but the purpose here is to test the unit commitment model against cases for which the actual data do not match the forecast, and thus the grid operator must use fast ramping units, dispatch reserves, call for demand management, etc., to address the unmet demand. This can be tested well with a forecast and an actual wind power that is generated from a realistic error analysis, as we propose here. We note that we have put tremendous care into modeling the variability and uncertainty of the energy generated from wind, with an energy model that captures the ramp rates of individual generators. We believe that our approach will produce a very accurate assessment of the ability to integrate significant levels of energy from wind.

Because the wind forecasting system used by PJM for their inland wind farms is provided by a contractor and is proprietary, we have limited knowledge of how the forecasts of wind speed and wind power were generated. We know that the model used is the WRF and that the forecast system ingests observations of wind speed and power taken at the inland wind farms in near real-time. Therefore, we would expect the PJM wind forecasting system to be advanced. Confirming that expectation, the PJM forecast system also exhibits good accuracy, with the median forecast error in wind power below 13% for individual wind farms and below 8% for all farms combined[2], based on our analysis of PJM inland data. The advantage of this approach is that we are basing the discrepancy between forecast and actual on a competitive commercial model based on WRF and used by a large RTO. The central assumption we are making is that our ability to forecast offshore wind, once all the turbines are installed (giving us the same access to actual data as we enjoy with onshore wind farms), will be the same as the current forecast errors for onshore wind farms over flat terrain, as supported by Foley et al. (2013).

The WRF setup, intended to mimic the real-time forecast operation, is described in the next subsection and its use to obtain the stochastic wind power forecast error model is described in section 3.

2.3 Wind forecasts with WRF

The WRF forecasts were run for the year 2010, because this was the year for which we had historical load and generation data from PJM. Since running both WRF and Smart-ISO models for an entire year would be computationally prohibitive, we focused on the months of January, April, July, and October, to capture the seasonal variability of both winds and loads, as was shown to be a valid approximation in Dvorak et al. (2010) for characterizing offshore wind resource in California. On each day of the four months, the WRF model was initialized at local noon and run for 48 hours with output every 10 minutes (details below). As such, two sets of WRF forecasts were available at each point of the domain on any given day: a 0-24-hour and a 24-48-hour forecast time series, with a 24-hour overlap. Because the time interval of interest is midnight-to-midnight each day and the forecasts must be completed by local noon, as dictated by the day-ahead market, the analysis in this paper focuses on the 12-36 hour forecasts from

[2] The 75th percentile was below 25% for single farms, and below 14% for all farms combined.

WRF. A total of 123 48-hour-long runs were carried out, which generated over 5 TB of output data; the WRF simulations used ~35,000 CPU-hours.

To mimic real-time forecast operation and reduce the horizon of each daily simulation to exactly 48 hours, as required by the SMART-ISO model, the WRF model was initialized as follows (Figure 2):

1. Initial conditions were provided by the NOAA North American Model (NAM) 12-km resolution forecasts valid at local noon (16:00 UTC during Daylight Saving Time and 17:00 UTC otherwise).

2. Boundary conditions were updated with the NAM forecasts every hour for the first 36 hours and every 3 hours for the last 12 hours.

3. WRF was initialized at local noon to coincide with the start of the day-ahead market in PJM. In order to complete the full 48-hour simulation by noon on each day, the WRF model would need to be started by 11 AM local time and therefore the NAM forecasts that were initialized at 12:00 UTC and valid at 16:00 or 17:00 UTC were used.

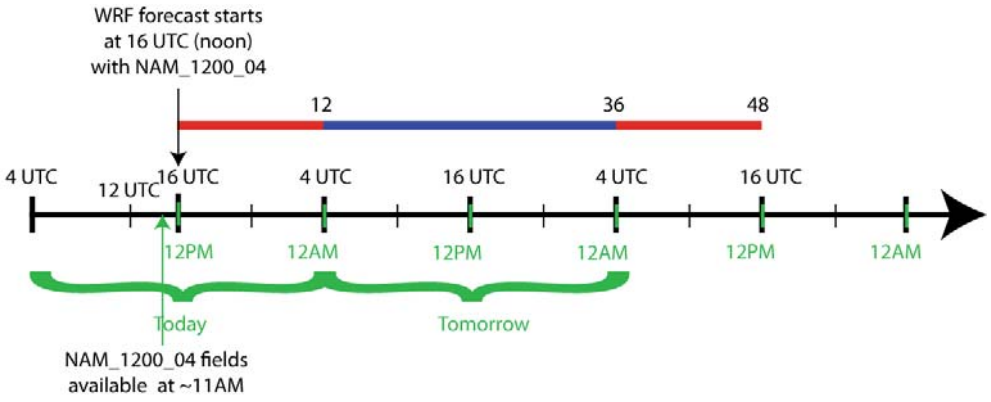

Figure 2: Timeline of the initialization and data acquisition for the WRF forecasts.

The WRF forecasts were generated using a previously validated WRF modeling configuration, used to generate the wind climatology for the U.S. East Coast in Dvorak et al. (2013). That study used two 5-km resolution domains to cover the entire eastern seaboard. Here we used the northern WRF domain from that study, which comprises 267x293 grid points spanning from North Carolina to Maine and goes no less than 400km offshore. The modeling domain extends sufficiently beyond the area of interest to limit the undesirable impacts of the lateral boundary conditions influencing the winds near boundaries. In the vertical, the default WRF configuration includes 41 levels, but additional vertical levels at heights of interest for validation and wind power forecasting (e.g., at 5 and 90 m) were added to the default set. Other WRF (version 3.3.1) configuration options were: Mellor-Yamada Nakanishi and Niino (MYNN) Level 2.5 planetary boundary layer scheme, the Kain-Fritsch cumulus parameterization scheme, and Monin-Obukhov surface layer physics.

Raw WRF output data were written in terrain-following pressure coordinates and post-processing was performed to output WRF wind fields at selected heights above sea level. In particular, wind fields were output at 90 m, the assumed turbine hub height. To obtain forecasts of wind power from 90-m wind

speed at all 29 blocks (Figure 1b), we used the power curve of the REpower 5 MW wind turbine from Dvorak et al. (2013).

The power P_k at block k at a given time is the sum of the power output of all $N_{i,j}$ wind turbines in each grid cell i,j belonging to block k, reduced by array losses of 10% (thus array efficiency η=0.90). The number of wind turbines in each cell is a function of the spacing between turbines, assumed here to be 10Dx10D, and of the fraction of each grid cell that belongs to each block. Because of the irregular shapes of the blocks, grid cells differ in count of installed turbines, thus making the calculation of the block power unnecessarily complicated. To simplify the calculation, the block-average wind speed was calculated first as follows:

$$\bar{V}_k = \frac{\sum_{(i,j)\in k} V_{i,j}}{n_k}, \qquad \textbf{Eq. 1}$$

where $V_{i,j}$ is the hub-height wind speed at grid cell i,j and n_k is the number of grid cells within block k. Next the block-average power per turbine $\bar{P}_k$ is calculated using the block-average wind speed from Eq. 1 in **Error! Reference source not found.** and then the block power P_k is obtained from:

$$P_k = N_k \eta \bar{P}_k, \qquad \textbf{Eq. 2}$$

where N_k is the total number of turbines in block k (Table I). This approximation introduces an error in the power calculation that on average causes a small negative bias (<1%) and adds a small amount of artificial variability (coefficient of variability is increased by 1.1-1.4%). Overall, the approximation is considered acceptable because it simplifies the post-processing of the data and contributes to making our results more conservative. For each of the five build-out levels, the total power generated is the sum of P_k from all the blocks that are included in that build-out level (Table I).

Time series of the total WRF forecast (or predicted) wind power by build-out level, for a week in each of the seasonal months, are presented side by side in Figure 3. In all seasons, periods of high wind power production alternate with periods of little to no production. The month of July has the longest period with no wind production and the month of October is characterized by the longest period of maximum generation.

Figure 3: Offshore wind power from WRF's 12-36 hr forecasts by build-out level for one week in each season.

The offshore wind power time series shown in Figure 3 are the 12-36 hr forecasts covering the midnight-to-midnight (local) time interval and initialized each day at noon, to mimic real-time operation. These 10-minute time series were used in the day-ahead unit commitment model of Smart-ISO, as described in Part II of this paper. For short-term forecasts, needed in the hour-ahead unit commitment and in the real-time economic dispatch models of Smart-ISO, we used persistence. In other words, in order to plan the short-term schedule of dispatchable generators (for the next, say, two hours), we use as forecasts the actual wind power (as noted above) twenty minutes *before* the start of the planning horizon. This value is held constant throughout the short-term planning horizon. As the short-term planning is done every half hour, the short-term forecasts are also updated every half hour.

3 The stochastic model of wind power forecast error

PJM provided proprietary time series of forecasted and actual wind power for all inland wind farms in the PJM area, between 2011 and January of 2014. The approximate geographical locations of those farms and of the proposed offshore wind farms are shown in Figure 4. As it can be seen, there are two main clusters of inland wind farms: one along the Appalachian Mountains, on the eastern portion of the PJM area, and another in the Great Plains, on the western portion of the area. In Figure 5 are also added the locations of the center points of our 29 blocks of offshore wind.

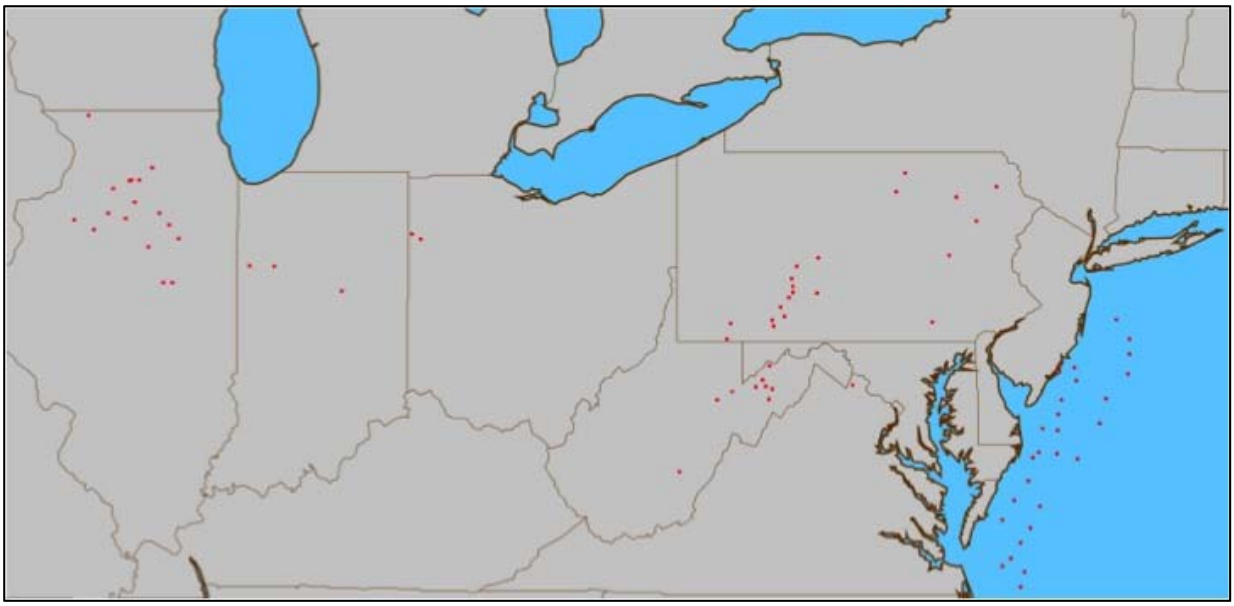

Figure 4: Approximate location of the PJM inland farms and of the proposed offshore wind farms.

Our goal is to simulate the power generation at the offshore wind farms, using the WRF forecasts obtained as described in section 2.3, combined with a stochastic model of the forecast error calibrated with the inland, or onshore, data. We propose the following methodology to accomplish this goal:

1. Choose one onshore wind farm over flat terrain and fit an auto-regressive, moving-average model (ARMA) to the time series of observed forecast errors for that farm.
2. Estimate the relationship between the correlation of forecast errors at two onshore farms and the distance between the farms.
3. Assume that the ARMA model calibrated in step 1 can be scaled to model the time series of forecast errors of each of the offshore wind farms. Foley et al. (2013) support our assumption that the performance of a forecasting system for offshore wind would be approximately as accurate as one for inland wind over flat terrain.
4. Assume that the correlation-to-distance relationship estimated in step 2 can be used to approximate the matrix of covariance of the offshore forecast errors.
5. Combine the ARMA models of the forecast errors at each of the offshore wind farms with the matrix of error covariance to generate multiple samples of forecast errors for the offshore farms.
6. Add the samples of forecast errors to the WRF forecasts in order to generate multiple simulations of the offshore wind power.

The first step in the methodology above required choosing onshore wind farms whose performance would best approximate the offshore wind farms. In terms of topography and wind dynamics, we considered that the cluster in the Great Plains would be the best fit. Consequently, we selected a subgroup of twenty-three farms from that cluster, comprised of those that were in operation during the entire months of January, April, July and October of 2013 (months we chose as representative months of the four seasons of the year), the most recent, complete year with PJM data. To evaluate the accuracy

of the forecasts for the selected subgroup of onshore farms, we computed several performance metrics of the total wind power forecasts. The results are depicted in Table II. Bias amplitudes are ~4.3% of the mean, RMSE ~40% of the mean, and correlations >0.8.

Table II: Performance metrics of the PJM proprietary 12-36 hour forecasts for onshore wind power during four months in 2013.

		Observed power		12-36 hr forecast power				
	N	Mean	Standard Deviation	Mean	Standard Deviation	Bias	RMSE	Correlation
		MW	MW	MW	MW	MW	MW	
January	4319	1,954	1,158	2,035	1,154	-81	488	0.913
April	4175	1,733	1,180	1,672	1,034	61	714	0.801
July	4319	579	537	619	517	-40	322	0.816
October	4319	1,154	827	1,266	812	-112	409	0.885

Although the total number of inland farms in the selected set (23) is comparable to the total number proposed for the offshore set (29), their sizes are significantly smaller, as indicated by the magnitude of the total power generation in Table II. In order to overcome this issue, we chose the largest onshore farm in the set, also referred to as the "control" wind farm, to provide the data to calibrate the stochastic model of the forecast error. This farm has an installed capacity around 0.5 GW, whereas the average installed capacity of the MAOWIT offshore blocks is about 2.5 GW (Table I). Furthermore, we calibrated a model for the relative forecast error, that is, the absolute forecast error expressed as a fraction of the installed capacity of the farm, so that it can be scaled to any of the (larger) offshore farms.

3.1 Calibration

We calibrated one stochastic error model for each season of the year. The procedure used in each case was the same and is outlined by the following steps:

1. Compute the cumulative empirical distribution (or histogram) of the relative forecast errors observed for *all* 23 onshore farms in the set.
2. Take the relative errors for the *control* onshore farm and transform them into Z-variates, first by mapping them to the corresponding fractions in the cumulative histogram computed in step 1, and then by using the inverse cumulative distribution of a Standard Normal.
3. The resulting Z-variate time series has data points every 10 minutes; extract a subset of this time series with data points every 20 minutes.
4. Fit an ARMA(5,1) model to the resulting 20-minutes spaced Z-variate time series. We note that the two parameters of the ARMA model (5 and 1) and the time gap between consecutive time series elements (20 minutes) were tuned by trial-and-error, until the simulated forecast errors were deemed close enough to the actual onshore forecast errors.

The ARMA model used here is defined as:

$$x[t] = a[1]x[t-1] + a[2]x[t-2] + \cdots + a[5]x[t-5] + e[t] + b[1]e[t-1], \qquad \textbf{Eq. 3}$$

where $\boldsymbol{x}$'s are the time series, $\boldsymbol{a}$'s are the auto-regressive coefficients, $\boldsymbol{b}$ is the moving average coefficient, and $\boldsymbol{e}$'s are the residuals. The calibrated values of the coefficients $\boldsymbol{a}$ and $\boldsymbol{b}$ and the resulting standard deviation $\boldsymbol{\sigma}$ of the fitted residuals are shown in **Table III**.

Table III: Coefficients of the calibrated ARMA(5,1) models and standard deviations of the fitted residuals by month in 2013.

Month-Year	$a[1]$	$a[2]$	$a[3]$	$a[4]$	$a[5]$	$b[1]$	σ
January	1.928	-1.059	0.118	-0.026	0.030	-0.861	0.359
April	0.429	0.551	-0.059	-0.009	-0.040	0.715	0.332
July	0.353	0.608	-0.142	0.130	-0.062	0.819	0.316
October	0.457	0.606	-0.235	0.011	0.036	0.778	0.322

Once calibrated, each ARMA model can then be used to generate samples of simulated errors over the appropriate planning horizon. Two remarks are in order here: (i) since the generated errors are expressed as Z-variates, they will have to be converted back to relative errors using the reverse sequence of step 2 above; and (ii) since a finer time grain is actually needed for the simulated error time series (data points every 10 minutes), linear interpolation will be used to generate the intermediate values.

We also found that, when doing the back conversion from generated Z-variates to relative errors, issues arose in the lower tail of the distribution of errors, because of the possibility of large negative errors translating into negative simulated power values. Truncating the values at zero introduced a bias in the distribution of simulated errors. This issue was mitigated by using, *in the back conversion only,* a set of conditional cumulative empirical error distributions, rather than the unconditional distribution computed in step 1. The distributions were conditioned on ranges of values of the WRF forecast errors. This issue was particularly relevant for the month of July, when the amount of wind available for power generation tends to be lower. We used ten ranges of values of WRF forecast relative errors to condition the cumulative error histograms in July: [0,…,0.01], (0.01,…,0.025], (0.025,…,0.05], (0.05,…,0.075], (0.075,…,0.1], (0.1,…,0.125], (0.125,…,0.15], (0.15,…,0.2], (0.2,…,0.25], (0.25,…,1].

3.2 Validation at the control onshore wind farm

To verify the accuracy of the calibrated stochastic error models, we generated 20 time series of equally-plausible forecast errors for the control onshore farm, for each month, and then compared them to the corresponding time series of actually observed forecast errors. The plots of simulated vs. observed forecast error histograms, for each month, are in Figure 5. The observed and simulated errors match each other closely and both are generally lower than 0.2 GW (with 0.5 GW of installed capacity). This suggests that 1) the current PJM forecast system is very accurate, and 2) our proposed ARMA predictions are reproducing the errors of the PJM forecast system correctly. July stands out as an especially well simulated month, with the highest frequency of small errors (about twice as high as the other months).

Figure 5: Histograms of the prediction errors at the control onshore PJM wind farm for the four months of interest in 2013.

Two additional metrics were used to infer the accuracy of the calibrated stochastic error models. They measure the pattern of oscillation of the actual time series above and below the forecasted series. One is defined as the number of consecutive time intervals that the forecast error is *positive* (that is, the observed time series is *above* the forecasted series). And the other is the number of consecutive time intervals that the forecast error is *negative* (that is, the observed time series is *below* the forecasted series). In Figure 6 we compare the cumulative histograms of the first metric for the observed and simulated series. In Figure 7 we compare the cumulative histograms for the second metric.

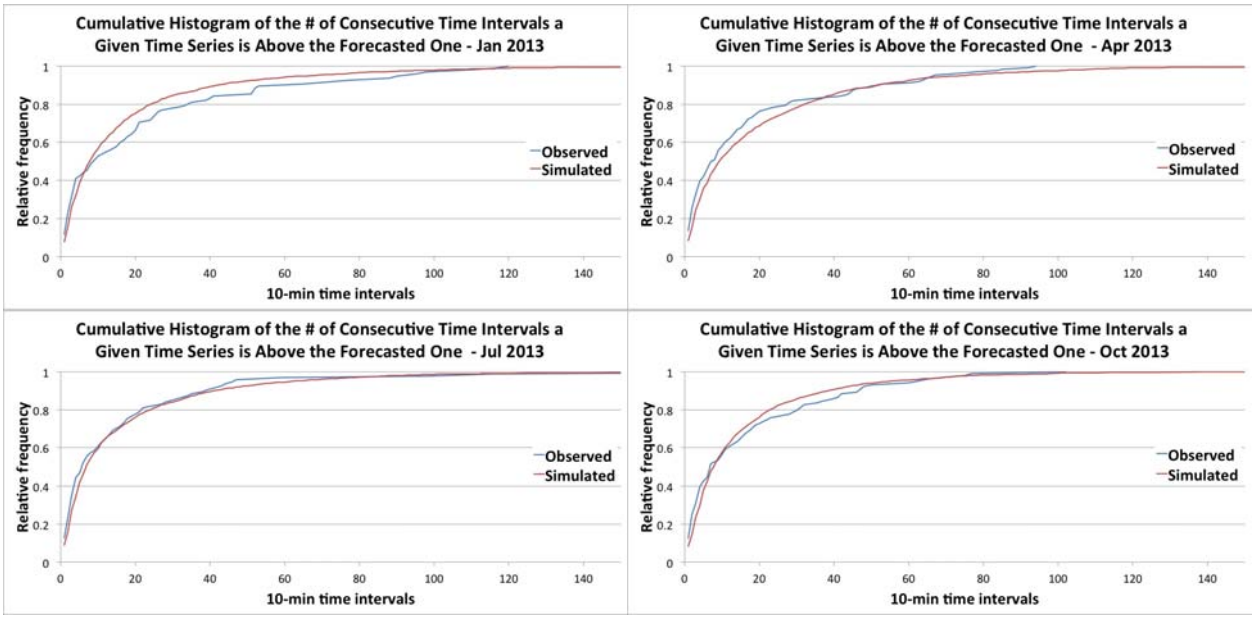

Figure 6: Cumulative histograms of the number of consecutive time intervals the forecast error is positive.

The plots in Figure 5, Figure 6 and Figure 7 show a good fit between the simulated and observed time series for the control onshore farm, in each of the seasons of the year, thus validating the calibrated stochastic error models used to generate the simulated time series.

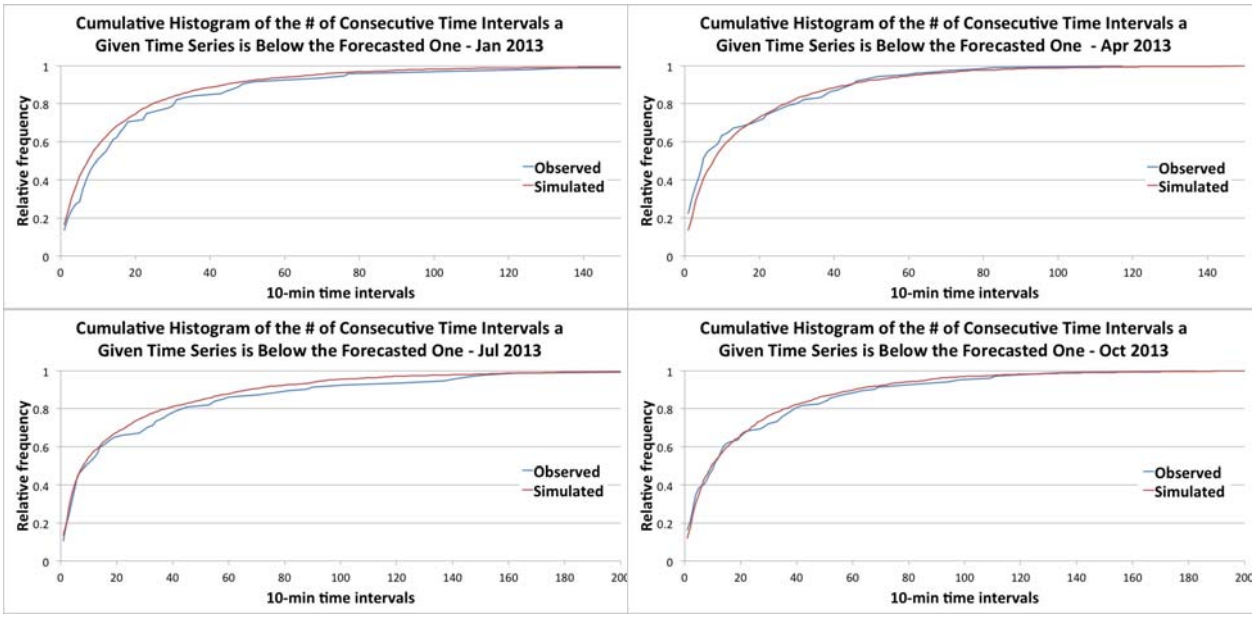

Figure 7: Cumulative histograms of the number of consecutive time intervals the forecast error is negative.

3.3 Accounting for spatial correlation

The next step in the proposed offshore wind power simulation methodology involved estimating the correlation between forecast errors at two wind farms as a function of the distance between those farms. This correlation of the forecast errors is expected to be generally positive and to decrease as the distance between the farms increases. We will use onshore data to estimate these functions and then assume that the functions will remain the same offshore. As mentioned earlier, this assumption of correlation of errors with distance is reasonable but it is neither supported nor denied by literature. For each season (or month), first we computed the matrix of forecast error correlation[3] between each pair of the 23 onshore farms in the Great Plains. Then, we fitted scaled exponential curves relating the correlation indices in the matrix with the distances between the pairs of farms. More specifically, we used the following functional form:

$$\rho = \gamma + (1-\gamma)e^{-\alpha d^{\beta}}, \qquad \textbf{Eq. 4}$$

where ρ is the correlation index between two farms, d is the distance in miles between them, and α, β and γ are parameters that were estimated for each season. The exponential coefficients α and β were estimated through a least squares procedure. The scaling factor γ was estimated through a linear search whose objective was to improve the overall matching between simulated and observed forecast errors

[3] We used correlation, rather than covariance, so that it can be extended to farms of a different scale (possibly larger).

aggregated over all farms for distances similar to those between our offshore blocks, up to ~200 km. Table IV shows the calibrated values for the parameters, while Figure 8 depicts the resulting correlation vs. distance functions.

Table IV: Parameters of the calibrated relationship between correlation of forecast errors and distance in 2013.

Month	α	β	γ
January	0.316	0.375	0.1
April	0.155	0.595	0.15
July	0.120	0.55	0.15
October	0.202	0.465	0.1

The final step in the offshore wind power simulation is to actually generate samples of forecast errors for all farms. The correlation-to-distance function is used to generate an approximation of the error correlation matrix between all pairs of farms in the desired set. The standard deviation σ from the ARMA model is combined with the approximate correlation matrix in order to yield the error *covariance* matrix Σ. Assuming that the forecast errors of the farms in the set follow a multivariate Normal distribution $N(X[t], \Sigma)$, where $X[t] = [x[t]]$ is the vector of expected errors at time t for all farms in the set, computed through the ARMA models, we can then generate multivariate samples of the forecast errors for all farms. Recall that these sampled errors are expressed as Z-variates of a cumulative empirical distribution (step 2 of the previously described procedure). They will have to be first appropriately converted back to relative forecast errors, and then scaled by the capacities of each farm in order to produce the final simulated absolute forecast errors.

Figure 8: Correlation of forecast errors at pairs of PJM inland wind farms as a function of the distance between wind farms.

3.4 Validation at all onshore wind farms

In order to verify the accuracy of the wind power simulation methodology as a whole, we generated 20 samples of forecast errors for all the 23 onshore farms in the Great Plains. We then compared the histograms of simulated forecast errors for all farms together with the histograms of actually observed forecast errors. Figure 9 displays these comparisons. The good match between simulated and observed histograms validate the proposed methodology and the calibration of the underlying models.

Figure 9: Histograms of the forecast (prediction) errors for all the PJM wind farms in the Great Plains together.

4 Results

Using the methodology described in the previous section in combination with the WRF forecasts described in subsection 2.3 we were able to generate seven sample paths of synthetic actual wind power which created a particular scenario in terms of weather shifts and storm patterns. We then used three different one-week-long blocks from those data, in each of the four months, in order to create a total of 7x3x4 = 84 sample paths representing different seasons, different meteorological conditions, and different sample realizations in terms of forecast errors.

We took the output from one of these instances and plotted the total wind power by build-out level in Figure 10, which can be compared to Figure 3. One can see that there are similar patterns between them, for each season of the year. But there are significant differences too, particularly in July.

Figure 10: Onshore-based wind power from one of the 21 equally-plausible scenarios considered in this study for each season by build-out level.

Perhaps a more interesting question is how the other equally-plausible actual time series compare with the WRF forecasts. We look at this question via Figure 11, where we plot the WRF forecasts (in black) and 5 onshore-based actuals (in different colors) for build-out level 5 every 10 minutes. A visual inspection of the plots in all months shows the variability present in the scenarios of synthetic actual wind.

Figure 11: WRF forecasted wind power and 5 equally-plausible, onshore-based, actual offshore wind power sample paths, at build-out level 5 for one week in each season.

Figure 12 shows the time series of forecasted (predicted) wind power over a portion of the simulation horizon in January, along with one of the simulated sample paths, for build-out level 5.

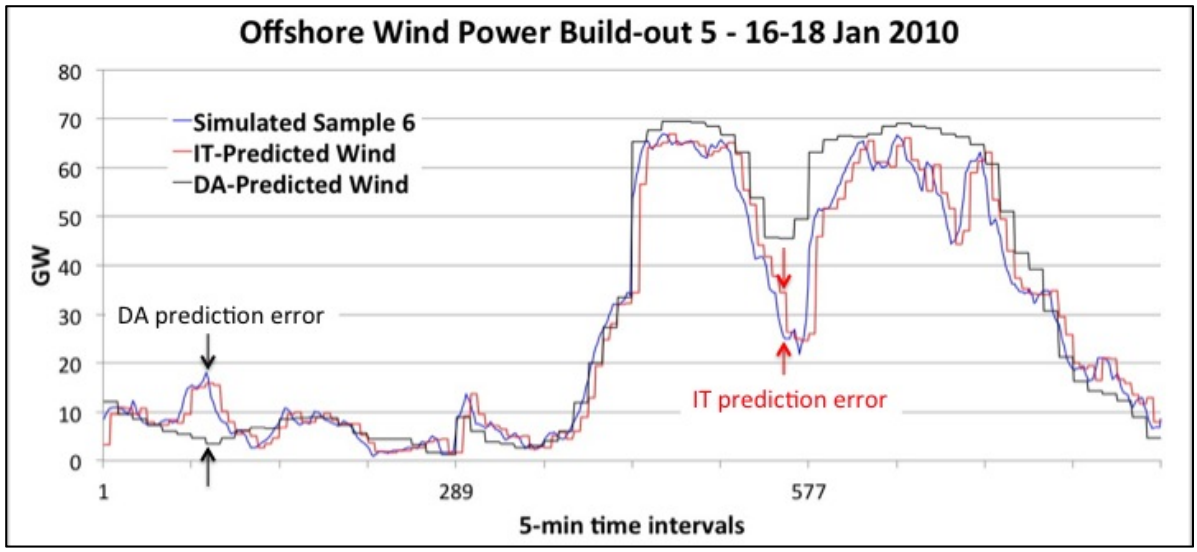

Figure 12: Intermediate-term (IT) and Day-Ahead (DA) errors when forecasting wind power.

The differences between the simulated power and the day-ahead forecasts constitute the day-ahead (DA) forecast errors, while the differences between simulated power and the intermediate-term forecasts constitute the intermediate-term (IT) forecast errors. Both types of errors are illustrated in Figure 12. Ideally, one would like to reduce these errors as much as possible. In our study, the DA forecast errors will be dealt with through the scheduling of fast generators in the intermediate-term unit commitment, whereas the IT forecast errors will be compensated by the use of (fast) reserves in the economic dispatch.

5 Conclusions

The purpose of this two-part study is to analyze the effects of large penetration of wind power in an RTO, using realistic wind inputs and a complete model of the power flow and unit commitment in the RTO. This paper describes the first part, the wind power forecast error model, whereas the accompanying second paper describes the power flow and unit commitment models and the overall results.

The chosen RTO is PJM Interconnection and the wind power is assumed to come from increasingly larger offshore wind farms located along the U.S. East Coast. Five build-out scenarios are studied, varying between 7 and 70 GW of installed capacity, considering exclusion zones and conflicting water uses. The wind forecasts are obtained via a current numerical weather prediction model, the WRF, but no offshore observations are available for validation or for generating wind power error statistics. Therefore we developed a stochastic wind forecast error model that uses historical wind forecast errors at inland PJM wind farms and applies them offshore to obtain stochastic time series of synthetic-actual offshore wind power.

Future offshore wind power development is likely to be accompanied by improved wind forecasting techniques, such as real-time data assimilation or rapid refresh. This study only uses existing forecasting

534 techniques. Current management practices are also utilized in this study and future, promising policies,
535 such as demand management or demand/response, are not considered. Therefore, the results of this
536 study are likely to be conservative.

537 6 Acknowledgments

538 This work was supported by the U.S. Department of Energy grant "Mid-Atlantic Offshore Wind
539 Interconnection and Transmission" (MAOWIT), Award Number DE-EE0005366. Mapping of conflict areas
540 and remaining blocks and sub-blocks was done by Blaise Sheridan and Regina McCormack.

541 7 References

542 Ahlstrom, M., D. Bartlett, C. Collier, J. Duchesne, D. Edelson, A. Gesino, M. Keyser, D. Maggio, M.
543 Milligan, C. Möhrlen, J. O'Sullivan, J. Sharp, P. Storck, and M. de la Torre Rodríguez, 2013: Knowledge Is
544 power: Efficiently integrating wind energy and wind forecasts. *IEEE Power and Energy Mag*, **11**, 45–52,
545 doi:10.1109/MPE.2013.2277999.

546 Apt, J., and P. Jaramillo, et al, 2014, Reduction of wind power variability through geographic diversity
547 (Chapter 12) in Apt and Jaramillo, *Variable Renewable Energy and the Electricity Grid*, RFF Press: New
548 York, NY.

549 Archer, C. L. and M. Z. Jacobson, 2003: The spatial and temporal distributions of U.S. winds and
550 windpower at 80 m derived from measurements. *Journal of Geophysical Research - Atmosphere*,
551 **108**(D9), doi:10.1029/2002JD0020076.

552 Archer, C. L. and M. Z. Jacobson, 2005: Evaluation of global wind power. *Journal of Geophysical Research*
553 *- Atmosphere*, **110**, D12110, doi:10.1029/2004JD005462.

554 Archer, C. L. and M. Z. Jacobson, 2007: Supplying baseload power and reducing transmission
555 requirements by interconnecting wind farms. *Journal of Applied Meteorology and Climatology*, **46**, 1701-
556 1717, doi:10.1175/2007JAMC1538.1.

557 Archer, C. L., B. A. Colle, L. Delle Monache, M. J. Dvorak, J. Lundquist, B. H. Bailey, P. Beaucage, M. J.
558 Churchfield, A. C. Fitch, B. Kosovic, S. Lee, P. J. Moriarty, H. Simão, R. J. A. M. Stevens, D. Veron, J.
559 Zackhttp, 2014: Meteorology for coastal/offshore wind energy in the United States: Recommendations
560 and research needs for the next 10 years. *Bulletin of the American Meteorological Society*, doi:
561 10.1175/BAMS-D-13-00108.1

562 Budischak, Cory, et al. "Cost-minimized combinations of wind power, solar power and electrochemical
563 storage, powering the grid up to 99.9% of the time." *Journal of Power Sources* 225 (2013): 60-74.

564 Cassola, Federico, et al. "Optimization of the regional spatial distribution of wind power plants to
565 minimize the variability of wind energy input into power supply systems." *Journal of Applied*
566 *Meteorology and Climatology* 47.12 (2008): 3099-3116.

567 Degeilh, Yannick, and Chanan Singh. "A quantitative approach to wind farm diversification and
568 reliability." *International Journal of Electrical Power & Energy Systems* 33.2 (2011): 303-314.

569 Delle Monache, L., and S. Alessandrini, 2014: Probabilistic wind and solar power predictions. *Renewable*
570 *Energy Integration*, 149-158.

571 Department of Energy (DOE), 2008: 20% wind energy by 2030. www.nrel.gov/docs/fy08osti/41869.pdf

572 Dvorak, M.J., C.L. Archer, and M.Z. Jacobson, 2010. California offshore wind energy potential. *Renewable*
573 *Energy*, doi:10.1016/j.renene.2009.11.022.

574 Dvorak, M. J., E. D. Stoutenburg, C. L. Archer, W. Kempton, and M. Z. Jacobson, 2012. Where is the ideal
575 location for a US East Coast offshore grid? *Geophysical Research Letters*, **39**, L06804,
576 doi:10.1029/2011GL050659.

577 Dvorak, M.J., B.A. Corcoran, J.E. Ten Hoeve, N.G. McIntyre, M.Z. Jacobson, 2013: U.S. East Coast offshore
578 wind energy resources and their relationship to peak-time electricity demand. *Wind Energy,* **16**(7), 977-
579 997, doi:10.1002/we.1524.

580 EnerNex Corporation, 2011: Eastern Wind Integration and Transmission Study, National Renewable
581 Energy Laboratory, Subcontract Report NREL/SR-550-47086, 241 pp., available at
582 http://www.nrel.gov/docs/fy11osti/47078.pdf

583 Foley, A. M., P. G. Leahy, A. Marvuglia, and E. J. McKeogh, 2012: Current methods and advances in
584 forecasting of wind power generation. *Renewable Energy*, **37**, 1–8, doi:10.1016/j.renene.2011.05.033.

585 Garvine, R. W., and W. Kempton, 2008: Assessing the wind field over the continental shelf as a resource
586 for electric power. *Journal of Marine Research*, **66**(6), 751-773.

587 GE Energy, 2010: Western Wind and Solar Integration Study, National Renewable Energy Laboratory,
588 Subcontract Report NREL/SR-550-47434, 535 pp., available at
589 http://www.nrel.gov/docs/fy10osti/47434.pdf

590 Hart, E. K., E. D. Stoutenburg, and M. Z. Jacobson, 2012: The potential of intermittent renewables to
591 meet electric power demand: Current methods and emerging analytical techniques. *Proceedings of the*
592 *IEEE*, **100**(2), 322-334.

593 Hirschberg, P. A., E. Abrams, A. Bleistein, W. Bua, L. Delle Monache, T. W. Dulong, J. E. Gaynor, B. Glahn,
594 T. M. Hamill, J. A. Hansen, D. C. Hilderbrand, R. N. Hoffman, B. H. Morrow, B. Philips, J. Sokich, and N.
595 Stuart, 2011: A weather and climate enterprise strategic implementation plan for generating and
596 communicating forecast uncertainty information. *Bull. Amer. Meteor. Soc.*, **12**, 1651–1666.

597 Kalnay, E., 2003: *Atmospheric modeling, data assimilation, and predictability*. Cambridge University
598 Press.

599 Katzenstein, W., E. Fertig, and J. Apt, 2010: The variability of interconnected wind plants. *Energy Policy*,
600 **38**(8), 4400-4410.

601 Kempton, W., C. L. Archer, A. Dhanju, R. W. Garvine, and M. Z. Jacobson, 2007: Large CO2 reductions via
602 offshore wind power matched to inherent storage in energy end-uses. *Geophysical Research Letters*, **34**,
603 L02817, doi:10.1029/2006GL028016.

604 Krishnamurti, T. N., C. M. Kishtawal, Z. Zhang, T Larow, D. Bachiochi, E. Williford, S. Gadgil, and S.
605 Surendran, 2000: Multimodel ensemble forecasts for weather and seasonal climate. *Journal of Climate*,
606 **13**, 4196–4216.

607 Leith, C. E., 1974: Theoretical skill of Monte Carlo forecasts. *Monthly Weather Review*, **102**, 409–418.

608 Lorenz, E. N., 1963: Deterministic non-periodic flow. *J. Atmos. Sci.*, **20**, 130–141.

609 Marquis, M., J. Wilczak, M. Ahlstrom, J. Sharp, A. Stern, J. C. Smith, and S. Calvert, 2011: Forecasting the
610 wind to reach significant penetration levels of wind energy. *Bull. Amer. Meteor. Soc.*, **92**, 1159–1171.

611 Molteni, F., R. Buizza, T. N. Palmer, and T. Petroliagis, 1996: The new ECMWF ensemble prediction
612 system: Methodology and validation. *Quart. J. Roy. Meteor. Soc.*, **122**, 73–119.

613 Naimo, A., 2014: A novel approach to generate synthetic wind data. *Procedia - Social and Behavioral*
614 *Sciences*, **108**, 187–196.

615 PJM, 2012: PJM 2012 Annual report, available at http://www.pjm.com/~/media/about-
616 pjm/newsroom/annual-reports/2012-annual-report.ashx

617 Sheridan, B., S. D. Baker, N. S. Pearre, J. Firestone, and W. Kempton, 2012: Calculating the offshore wind
618 power resource: Robust assessment methods applied to the U.S. Atlantic Coast. *Renewable Energy*, **43**,
619 224-233. doi:10.1016/j.renene.2011.11.029.

620 Simão, H., W. Powell, C. L. Archer, and W. Kempton, 2015: The challenge of integrating wind power in
621 the U.S. electric grid. Part II: Simulation of the PJM market operation. *Renewable Energy*, submitted.

622 Skamarock, W.C., J. B. Klemp, J. Dudhia, D. O. Gill, D. M. Barker, M. G. Duda, X. Huang, W. Wang, and J. G
623 Powers, 2008: A description of the Advanced Research WRF version 3. *Technical Report NCAR/TN–*
624 *475+STR*, NCAR, available at http:// www.mmm.ucar.edu/wrf/users/docs/arw_v3.pdf.

625 Soder, L, 2004: Simulation of wind speed forecast errors for operation planning of multiarea power
626 systems. Proceedings of the 2004 International Conference on Probabilistic Methods Applied to Power
627 Systems, Ames (IA), 723-728.

628 Toth, Z., and E. Kalnay, 1993: Ensemble forecasting at NMC: The generation of perturbations. *Bull. Am.*
629 *Meteorol. Soc.*, **74**, 2317–2330.

630 Toth, Z., and E. Kalnay, 1997: Ensemble forecasting at NCEP: The breeding method. *Mon. Wea. Rev.*,
631 **125**, 3297–3319.

632 Ummels, B. C., M. Gibescu, E. Pelgrum, W. L. Kling, and A. J. Brand, 2007: Impacts of wind power on
633 thermal generation Unit Commitment and dispatch. *IEEE Transactions on Energy Conversion*, **22**(1), 44-
634 51.

635 U.S. Department of Energy (DOE), 2008: 20% wind energy by 2030: Increasing wind energy's
636 contribution to U.S. electricity supply. *NREL Rep. TP-500-41869, DOE/GO-102008-2567*, 248 pp.,
637 available at http://www.nrel.gov/docs /fy08osti/41869.pdf.

638